$Cu_2ZnSnSe_4$ device obtained by formate chemistry for metallic precursor layer fabrication

Sara Tombolato [a,*], Ulrich Berner [b,c], Diego Colombara [b], Daniel Chrastina [d], Markus Widenmeyer [c], Simona O. Binetti [a], Phillip J. Dale [b]

[a] *Department of Materials Science and Solar Energy Research Center (MIB-SOLAR), University of Milano-Bicocca, via Cozzi 53, Milan, Italy*
[b] *Laboratory for Energy Materials, Physics and Material Science Research Unit, Université du Luxembourg, 41, rue du Brill, L-4422, Luxembourg*
[c] *Robert Bosch GmbH, Corporate Sector Research and Advance Engineering, Applied Research Chemistry (CR/ARC), Robert Bosch Platz 1, D-70839 Gerlingen-Schillerhöhe, Germany*
[d] *L-NESS, Department of Physics, Politecnico di Milano, Polo di Como, via Anzani 42, I-22100 Como, Italy*

Received 15 December 2014; received in revised form 12 March 2015; accepted 16 March 2015

1. Introduction

Kesterites are becoming one of the most studied family of compounds among thin film absorbers in the photo-voltaic field. The class includes all the alloys with the min-imum formula $Cu_2(Fe, Zn)(Sn, Ge)(S, Se)_4$. They are characterized by band gaps and absorption coefficients very similar to those of $CuIn_xGa_{(1-x)}Se_2$ (CIGS) but the constituent elements are of higher earth abundance (Repins et al., 2011).

To achieve the terawatt-scale power generation with photovoltaics, these materials need to be produced in an easy and scalable way, thus many groups are concentrating on kesterite precursor layers formation by non-vacuum or so-called "wet processes" (Romanyuk et al., 2013). In most cases they involve solutions or suspensions which contain all the metallic constituents; this condition should favor their homogenous alloying during the formation of the precursor layer, because the intermixing happens at a molecular level. The resulting absorber layers produced by wet processes are usually characterized by contamination arising from solvents or reagents used for the ink preparation, even though the high temperatures usually involved in the fabrication of the absorbers should ensure solvent

* Corresponding author.
E-mail address: s.tombolato@campus.unimib.it (S. Tombolato).

evaporation and thermolysis of organic residue. Halides, nitrogen, oxides and, of course carbon are the main species that can be found in a kesterite thin film grown by direct solution deposition (Rajeshmon et al., 2011).

Nonetheless, the CZTSSe device efficiency record of 12.7% is held by the IBM laboratories (Kim et al., 2014), with the absorber produced by a non-vacuum solution approach that involves hydrazine. Hydrazine (N_2H_4) is a powerful reducing agent that, in presence of excess chalcogen (S, Se, Te), can solvate different metal chalcogenides as hydrazinium-based complexes at room temperature (Yuan and Mitzi, 2009). Its controlled degradation produces N_2 and H_2 only, which are gaseous products that are released during thermal treatment and thus should not leave any contaminant in the CZTSSe film. Because of its high toxicity and flammability, finding alternatives with a high solvating power, reducing capability and "clean" products upon degradation is highly desirable. The design of "green" fabrication techniques is a very relevant topic nowadays, also in other PV technologies, and many examples can be found in the literature (Chiappone et al., 2014; Chen et al., 2014). Recently, a paper describing the fabrication of CIGS thin films by means of metal formate chemistry has been published (Berner and Widenmeyer, 2014). It uses a mixture of a nitrogen containing base (1,1,3,3 - tetramethylguanidine) and an alcohol (CH_3OH) as solvents and the formates of copper, indium and gallium as elemental sources. The formate group upon heating reduces metallic cations (M) involved in the precursor layer preparation, and its oxidation under inert atmosphere releases CO_2 and H_2 according to the reaction: $M(HCOO)_n(s) \rightarrow M(s) + nCO_2(g) + \frac{n}{2} H_2(g)$. H_2 is a reducing agent itself and can protect the metals against reoxidation (Brauer, 1963). In this paper we are presenting a similar route applied to CZTSe. A concentrated ink containing Cu and Zn formates and Sn methoxide is formulated and deposited, giving continuous precursor layers. The resulting absorber layers are characterized and initial solar cell results are reported.

2. Experimental

Copper and zinc formates were produced by the reaction of the respective nitrates ($Cu(NO_3)_2{\cdot}xH2O$ 99.999%, $Zn(NO_3)_2{\cdot}6H2O$ $\geqslant$99.0% both Sigma Aldrich) with formic acid (Sigma Aldrich, ACS reagent $\geqslant$96.0%) in air, while the source for tin was the methoxide (anhydrous, Alfa Aesar), used with no further purification, as solvents 1,1,3,3 - tetramethylguanidine (TMG) and methanol (both from abcr, 99%) were used. Tin (II) selenide and elemental selenium pellets (both 99.999% pure) were purchased from Alfa Aesar. Since $Sn(OCH_3)_2$ and the TMG decompose quickly in the presence of water, the whole ink preparation and deposition were conducted inside a nitrogen filled glove box. The substrate for the deposition was soda-lime-glass on which a 700 nm thick layer of molybdenum was sputtered. The latter is one of the most common back contacts used for the building of CZTSe solar cells. The ink formulation proceeds as follows:copper formate, zinc formate and tin methoxide are mixed in a 3 ml vial and dissolved in a mixture of TMG and methanol (respectively 45% and 55% wt%) so that the weight percentage of salts in solution is around 25%.

The vial is kept on a hot plate set at 105 °C under stirring for a couple of minutes. Methanol is periodically added to compensate for its evaporation. The appearance of the solution just before it was deposited is shown in Fig. 1.

The ink was deposited at a speed of 15 mm/s using a Zehner ZAA 2300 automatic film applicator and a ZUA 2000 universal applicator with a gap above the substrate of 350 μm. Immediately after deposition, the samples were placed on a hot plate set at 140 °C and the temperature was raised each 10 min by 10 °C up to 200 °C and kept at this temperature for 10 min in order to remove any organic residue and obtain the pure metallic components.

The precursor layers were converted into CZTSe in a tubular furnace. They were placed in a graphite box inside a quartz tube together with 100 mg of elemental selenium and 15 mg of SnSe. In a typical experiment both the samples and the sources of selenium and tin are kept at the same temperature (550 °C) with 10 mbar of forming gas for 30 min. The system was then allowed to cool naturally.

In order to build the photovoltaic device, the samples were etched in a 5 wt% KCN aqueous solution for 30 s and put in the chemical bath to deposit CdS on top of them. Intrinsic ZnO and Al doped ZnO were deposited via magnetron sputtering followed by e-beam evaporation of Ni–Al grids. Solar cells with a total area of 0.5 cm^2 were scribed mechanically.

Top-view and cross-section SEM micrographs were collected with a Hitachi SU-70 and a Tescan VEGA TS5136XM. The elemental compositions of the precursor and selenized films were investigated with EDX in sample areas of 120 by 90 μm. The Raman spectra were collected at room temperature with a Jasco Ventuno micro-Raman

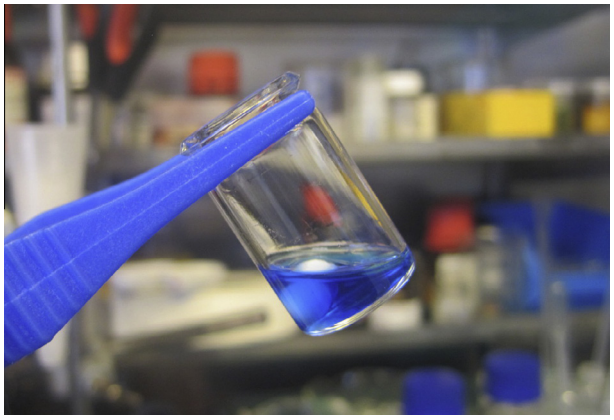

Fig. 1. Vial containing the ink used for the deposition of the three metals.

spectrometer in backscattering configuration using a helium–neon laser with a power of around 7 mW (spot diameter ≈ 4 μm). The thickness of the film was measured with a Veeco Dektak 8 profilometer, equipped with a stylus with radius of 12 μm. C and N content in the selenized powdered films were detected with a Elementar vario MICRO cube. The films were also analyzed by X-ray diffraction in ω–2θ configuration using a PANalytical X'Pert PRO MRD high-resolution diffractometer with a Cu $K\alpha_1$ radiation source (wavelength $\lambda = 0.154$ nm) at 45 kV and 40 mA. A home-built I–V setup equipped with an AM1.5 intensity equivalent calibrated halogen lamp (100 mW/cm^2) was used to measure I–V characteristics in the dark and under illumination. The external quantum efficiency (EQE) measurements were performed on a home-built setup calibrated with a Si and an InGaAs photodiode. The photocurrent was measured by using chopped monochromatic illumination from xenon and tungsten lamps and a lock-in amplifier was used to measure the photocurrent.

3. Results and discussion

Since the best CZTS solar cells in the literature have been produced with Cu-poor and Zn-rich absorber layers (Tanaka et al., 2010), we formulated the ink accordingly. The typical elemental ratios of the ink and selenized films are reported in Table 1. The elemental composition of the precursor layers after drying at 200 °C depends on the region investigated. As can be noticed from Fig. 2, the layer is composed of aggregates of sub-micrometer particles embedded in an organic matrix. On top of the layer, some rounded particles with a diameter in the order of 2 μm are present. EDX measurement of the aggregates revealed the presence of the three metals, as well as carbon and oxygen, while the shiny rounded particles were composed of mainly copper, carbon and oxygen.

The thickness of the layer is around 700 nm. EDX measurements collected on different areas of the selenized films reveal elemental ratios very close to $Cu_2ZnSnSe_4$ stoichiometry, indicating a loss of zinc compared to the quantity introduced in the ink. As Cu is not in excess, no Sn can be absorbed from the atmosphere, so the Zn depletion must be related to elemental Zn loss before selenization (Washburn and West, 1926). Nevertheless, different EDX point measurements at 7 kV on the brighter areas (as highlighted inside the oval in Fig. 3) showed a composition poor in Cu and Zn-rich: $\frac{Cu}{Zn+Sn} = 0.60, \frac{Zn}{Sn} = 3.0$, with ZnSe

Table 1
Compositional ratios in the ink and selenized film.

	Elemental composition expressed as ratios of atomic percentages	
	Ink	Selenized film
$\frac{Cu}{Zn+Sn}$	0.82 ± 0.02	0.86 ± 0.07
$\frac{Zn}{Sn}$	1.20 ± 0.04	0.96 ± 0.04

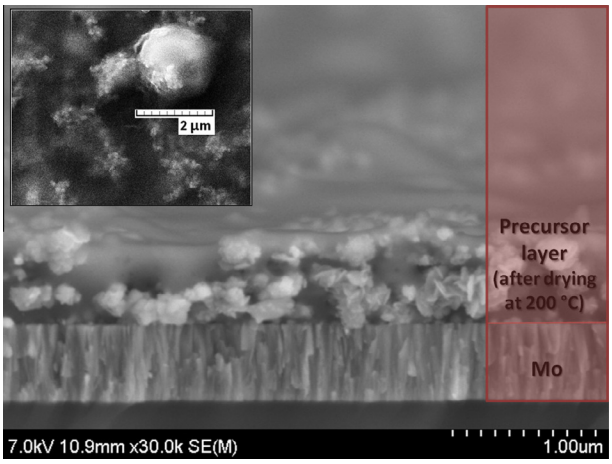

Fig. 2. SEM micrograph of the cross section of a precursor layer deposited on molybdenum. Inset: top view of the same layer.

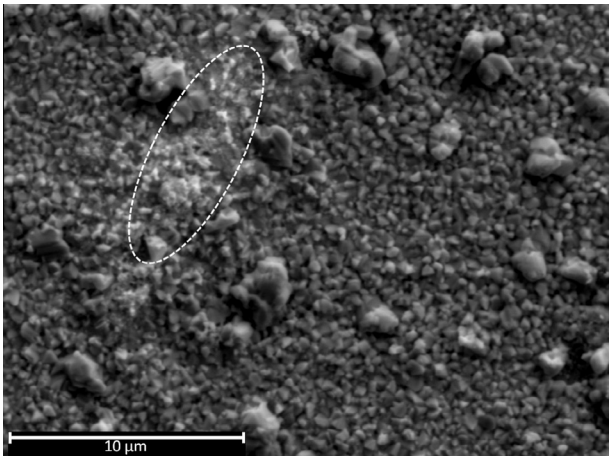

Fig. 3. Low magnification top-view SEM micrograph of the selenized film. The highlighted area is characterized by a Zn-rich composition according to EDX measurements.

being the most probable secondary phase on the surface portion analyzed.

From high magnification top view SEM micrographs (Fig. 4a), the CZTSe film appears composed of angular-shaped crystals with dimensions of around 500 nm and some bigger grains with the same composition, resulting in an overall compact microstructure with some pinholes. The SEM cross section shows a double-layered film with a layer of small grains attached to the molybdenum sele-nide (Fig. 4b). Other groups reported a similar layer sand-wiched between $MoSe_2$ and the selenized absorber and attributed it to a carbon rich material (Cao et al., 2012; Ilari et al., 2012). It has also been shown for CZTSSe devices that the efficiency is influenced by the thickness of this carbon rich layer, which can be decreased by optimis-ing the selenization conditions so that it does not inhibit efficient operation of the cell (Miskin et al., 2014).

The mechanical removal of the bilayer was not feasible because it was solidly attached to the $MoSe_2$ which was

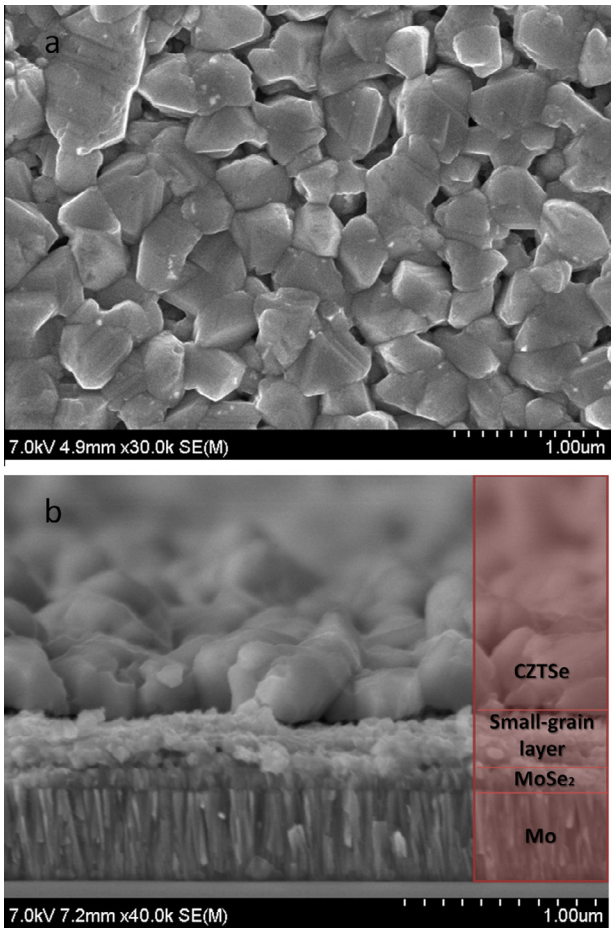

Fig. 4. High magnification SEM pictures of the top-view (a) and tilted cross-section (b) of a selenized sample.

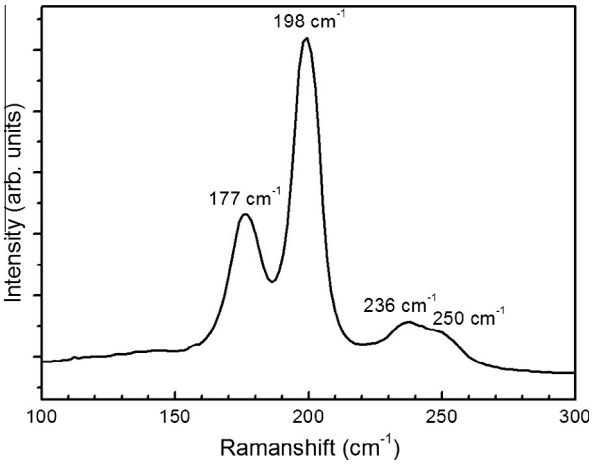

Fig. 5. Raman spectrum of the absorber layer using a 632.8 nm laser as excitation source. Estimated penetration depth: 350 nm.

itself very strongly bound to the metallic molybdenum, thus there was no chance to analyze the layer underneath the CZTSe by Raman spectroscopy. The overall film thick-ness measured with the profilometer was 1.1 μm.

The elemental analysis of the powder obtained by scratching the film deposited on a microscope slide revealed very low carbon and nitrogen contents (0.18 ± 0.05 and 0.54 ± 0.1 wt%), compared with their mass percentage in the ink (35.59% and 12.39% respectively), meaning that the decomposition of solvents and reagents occurred with-out leaving any significant contamination in the film. According to this compositional analysis, we can estimate that there is one carbon atom for each five CZTSe unit cells. The same analysis was carried out previously on CIGS grown in Berner and Widenmeyer (2014), where C and N amounts were 0.07 and 0.15 wt%, values signifi-cantly lower than in these CZTSe samples, probably because of a more accurate design of the drying step after deposition.

In order to examine the surface of the film further, Raman spectra were collected at several locations of the film and they all resemble that reported in Fig. 5, implying a good degree of chemical homogeneity. Peaks at 198 cm^{-1}, 177 cm^{-1}, 236 cm^{-1} and 250 cm^{-1} indicate that CZTSe is the main crystalline phase in the samples (He et al., 2014), no evidence of other binary or ternary phases is found from this analysis. Surface ZnSe was observed in the SEM image of the absorber but is not seen in the Raman spectra since the 632.8 nm laser does not suffi-ciently interact with it (Djemour et al., 2013).

In order to analyze the crystal structure of the absorber layer, an XRD analisys was carried out. In Fig. 6 the XRD patterns with the as-collected (a) and logarithmic intensities (b) are presented, respectively. The majority of signals belong to the $Cu_2ZnSnSe_4$ kesterite structure (PDF – 04-003-8817). The diffraction peak corresponding to the (1 1 2) plane located at 27.14° was fitted with a Gaussian, and the full-width at half-maximum (FWHM) is 0.31°(inset of Fig. 6a). This diffraction peak was used in the Scherrer equation to determine the mean crystallite size of the CZTSe phase, which was found to be 279 ± 4 nm. The value is consistent with sizes observed in the SEM micrographs. It can also be noted that from these measure-ments that the presence of cubic ZnSe cannot be excluded and signals coming from metallic molybdenum under the absorber layer are visible.

The highest efficiency achieved for a solar cell produced with the absorber layer described here is 2.39%. Its current density–voltage characteristics is shown in Fig. 7a and the external quantum efficiency (EQE) is depicted in Fig. 7b. The low Fill Factor (FF) and open-circuit voltage (V_{oc}) are typical features of a highly defective material. It is dif-ficult to ascertain whether the recombination centres are located at the interface of the material with the small-grain layer, or at the boundaries of CZTSe grains or in the bulk of the grains. Furthermore the best device exhibits only a small shunt resistance and a large series resistance. The J_{sc} was extracted from the J–V curve under illumination and from the integration of the EQE curve, giving respec-tively values of 31.2 mA cm^{-2} and 32.7 mA cm^{-2}, which

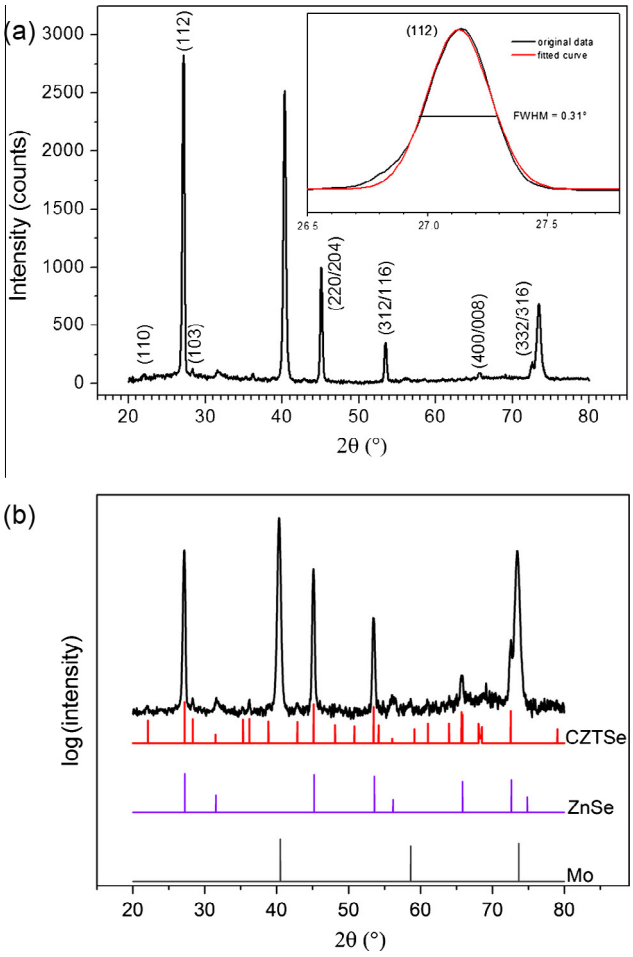

Fig. 6. XRD patterns of $Cu_2ZnSnSe_4$ thin films grown on molybdenum.(a) Diffracted intensities as collected and (inset) Gaussian fitting of the (1 1 2) peak used in the Scherrer equation to determine grain size, (b) plot of the logarithm of intensities of the experimental data and simulated patterns taken from the ICDD database (PDF CARDS: $Cu_2ZnSnSe_4$ 04-003-8817, ZnSe 00-037-1463, Mo 00-042-1120).

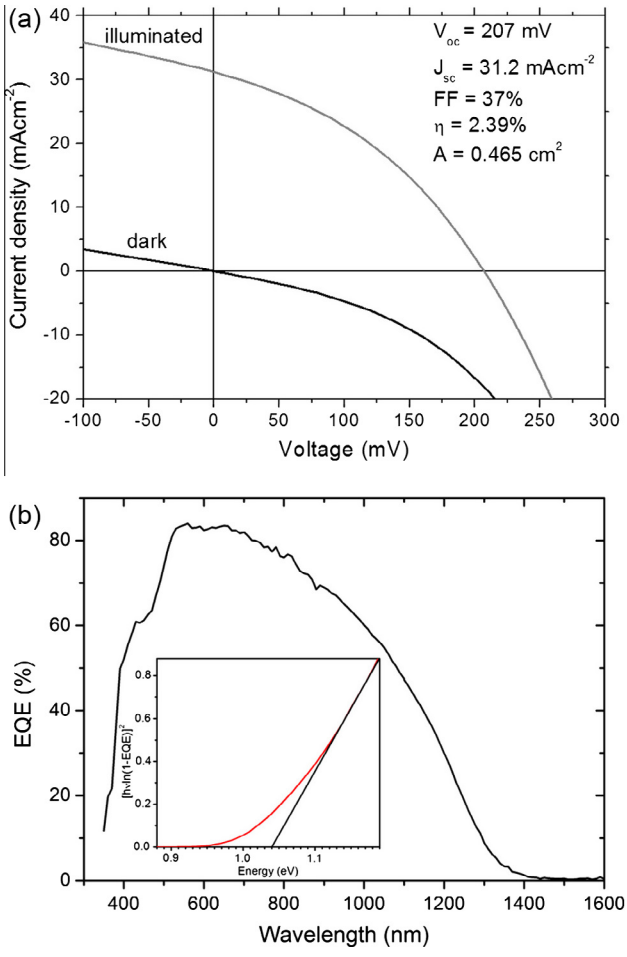

Fig. 7. (a) *J–V* curve and (b) corresponding EQE of the best solar cell. Inset shows the plot of $[h\nu \cdot \ln(1 - \mathrm{EQE})]^2$ against the photon energy, which gave an estimation of the optical bandgap (1.04 eV).

match quite well with some much more efficient CZTSe cells reported in the literature (Repins et al., 2012; Shin et al., 2012).

From the linear fit of the low energy part of the plot $[h\nu \cdot \ln(1\text{-EQE})]^2$ against photon energy, the bandgap of CZTSe was extrapolated and found to be around 1.04 eV (inset of Fig. 7b) which is indicative of an ordered kesterite structure, consistent with the slow cooling the samples underwent after the selenization step (Rey et al., 2014). Recently, Colombara et al. showed that the shape and magnitude of the EQE is related to the number and size of ZnSe islands on the surface of the CZTSe absorber layer (Colombara et al., 2014). In this respect the reasonably high overall quantum efficiency, especially in the (blue) region of ZnSe optical absorption, points to a low concen-tration of ZnSe on the surface, with presumably smaller size compared to the effective diffusion length of the minor-ity carriers. The low concentration of ZnSe is in line with the almost stoichiometric composition measured by EDX.

4. Conclusions

Polycrystalline CZTSe was obtained by means of formate chemistry plus selenization at 550 °C. A quantification of the carbon over CZTSe unit cells has been shown, but the effects of this presence and its exact location still need to be clarified.

Functioning devices were built with these absorbers and their performance is promising for further study. Among the possible pathways to improve cell efficiency, three stand out. Firstly the Zn content of the final absorber layer should be increased slightly to remove any possibility of forming the Cu_2SnSe_3 phase which is known to be detri-mental to device performance. Secondly, an improved annealing routine is required to remove the final carbon and nitrogen residues which are speculated to be detrimen-tal to the devices performance. Thirdly, sodium addition to the absorber is known to enhance V_{oc} and FF in other solu-tion processed CZTSe absorber layers (Sutter-Fella et al., 2014).

Acknowledgements

Sara Tombolato would like to thank Dr. Andrea Scaccabarozzi of MIB-SOLAR for giving insightful comments and suggestions. Diego Colombara and Phillip Dale acknowledge the EU seventh framework programme FP7/2007-2013 for funding through the Grant no. 284486.

References

Berner, U., Widenmeyer, M., 2014. Solution-based processing of Cu(In, Ga)Se_2 absorber layers for 11% efficiency solar cells via a metallic intermediate: solution-based processing of CIGS absorber layers. Prog. Photovoltaics Res. Appl. http://dx.doi.org/10.1002/pip.

Brauer, G., 1963. Handbook of Preparative Inorganic Chemistry, Second ed. Academic Press-Elsevier, London – New York.

Cao, Y., Denny, M.S., Caspar, J.V., Farneth, W.E., Guo, Q., Ionkin, A.S., Johnson, L.K., Lu, M., Malajovich, I., Radu, D., Rosenfeld, H.D., Choudhury, K.R., Wu, W., 2012. High-efficiency solution-processed $Cu_2ZnSn(S, Se)_4$ thin-film solar cells prepared from binary and ternary nanoparticles. J. Am. Chem. Soc. 134, 15644–15647.

Chen, P.-Y., Qi, J., Klug, M.T., Dang, X., Hammond, P.T., Belcher, A.M., 2014. Environmentally responsible fabrication of efficient perovskite solar cells from recycled car batteries. Energy Environ. Sci. 7, 3659–3665.

Chiappone, A., Bella, F., Nair, J.R., Meligrana, G., Bongiovanni, R., Gerbaldi, C., 2014. Structure-performance correlation of nanocellulose-based polymer electrolytes for efficient quasi-solid DSSCs. Chemelectrochem 1, 1350–1358.

Colombara, D., Robert, E.V.C., Crossay, A., Taylor, A., Guennou, M., Arasimowicz, M., Malaquias, J.C.B., Djemour, R., Dale, P.J., 2014. Quantification of surface ZnSe in $Cu_2ZnSnSe_4$-based solar cells by analysis of the spectral response. Sol. Energy Mater. Sol. Cells 123, 220–227.

Djemour, R., Mousel, M., Redinger, A., Gütay, L., Crossay, A., Colombara, D., Dale, P.J., Siebentritt, S., 2013. Detecting ZnSe secondary phase in $Cu_2ZnSnSe_4$ by room temperature photoluminescence. Appl. Phys. Lett. 102, 222108.

He, J., Tao, J., Meng, X., Dong, Y., Zhang, K., Sun, L., Yang, P., Chu, J., 2014. Mater. Lett. 126, 1–4.

Ilari, G.M., Fella, C.M., Ziegler, C., Uhl, A.R., Romanyuk, Y.E., Tiwari, A.N., 2012. Solar cell absorbers spin-coated from amine-containing ether solutions. Sol. Energy Mater. Sol. Cells 104, 125–130, set. 2012.

Kim, J., Hiroi, H., Todorov, T.K., Gunawan, O., Kuwahara, M., Gokmen, T., Nair, D., Hopstaken, M., Shin, B., Lee, Y.S., Wang, W., Sugimoto, H., Mitzi, D.B., 2014. High efficiency $Cu_2ZnSn(S, Se)_4$ solar cells by applying a double In_2S_3/CdS emitter. Adv. Mater. 26, 7427–7431.

Miskin, C.K., Yang, W.-C., Hages, C.J., Carter, N.J., Joglekar, C.S., Stach, E.A., Agrawal, R., 2014. 9.0% efficient $Cu_2ZnSn(S, Se)_4$ solar cells from selenized nanoparticle inks. Prog. Photovoltaics Res. Appl. http://dx.doi.org/10.1002/pip.

Rajeshmon, V.G., Kartha, C.S., Vijayakumar, K.P., Sanjeeviraja, C., Abe, T., Kashiwaba, Y., 2011. Role of precursor solution in controlling the opto-electronic properties of spray pyrolysed Cu_2ZnSnS_4 thin films. Sol. Energy 85, 249–255.

Repins, I., Vora, N., Beall, C., Wei, S.-H., Yan, Y., Romero, M., Teeter, G., Du, H., To, B., Young, M., Noufi, R., 2011. Kesterites and chalcopyrites: a comparison of close cousins. MRS Proceedings 1324, pp. 1311–1324.

Repins, I., Beall, C., Vora, N., DeHart, C., Kuciauskas, D., Dippo, P., To, B., Mann, J., Hsu, W.-C., Goodrich, A., Noufi, R., 2012. Co-evaporated $Cu_2ZnSnSe_4$ films and devices. Sol. Energy Mater. Sol. Cells 101, 154–159.

Rey, G., Redinger, A., Sendler, J., Weiss, T.P., Thevenin, M., Guennou, M., El Adib, B., Siebentritt, S., 2014. The band gap of $Cu_2ZnSnSe_4$: effect of order-disorder. Appl. Phys. Lett. 105, 112106.

Romanyuk, Y.E., Fella, C.M., Uhl, A.R., Werner, M., Tiwari, A.N., Schnabel, T., Ahlswede, E., 2013. Recent trends in direct solution coating of kesterite absorber layers in solar cells. Sol. Energy Mater. Sol. Cells 119, 181–189.

Shin, B., Zhu, Y., Bojarczuk, N.A., Jay Chey, S., Guha, S., 2012. Control of an interfacial $MoSe_2$ layer in $Cu_2ZnSnSe_4$ thin film solar cells: 8.9% power conversion efficiency with a TiN diffusion barrier. Appl. Phys. Lett. 101, 053903.

Sutter-Fella, C.M., Stückelberger, J.A., Hagendorfer, H., La Mattina, F., Kranz, L., Nishiwaki, S., Uhl, A.R., Romanyuk, Y.E., Tiwari, A.N., 2014. Sodium assisted sintering of chalcogenides and its application to solution processed $Cu_2ZnSn(S, Se)_4$ thin film solar cells. Chem. Mater. 26, 1420–1425.

Tanaka, T., Yoshida, A., Saiki, D., Saito, K., Guo, Q., Nishio, M., Yamaguchi, T., 2010. Influence of composition ratio on properties of Cu_2ZnSnS_4 thin films fabricated by co-evaporation. Thin Solid Films 518, S29–S33.

Washburn, E.W., West, C.J., 1926. International Critical Tables of Numerical Data, Physics, Chemistry and Technology. McGraw-Hill Book Company Inc., New York., Published for the National Research Council.

Yuan, M., Mitzi, D.B., 2009. Solvent properties of hydrazine in the preparation of metal chalcogenide bulk materials and films. Dalton Trans. 31, 6078–6088.